Journal of Constructional Steel Research 205 (2023) 107895

Contents lists available at ScienceDirect

Journal of Constructional Steel Research

journal homepage: www.elsevier.com/locate/jcsr

Development of small-scale buckling-restrained brace analog for physical experiments of structural systems

Nicholas E. Wierschem [a,*], Lindsay Kirk [b], Mark D. Denavit [a]

[a] Department of Civil and Environmental Engineering, University of Tennessee, Knoxville, TN 37996, United States of America
[b] Haines Structural Group, Knoxville, TN, United States of America

ARTICLE INFO

Keywords:
Buckling restrained brace
Small-scale
Experimental hardware
Empirical equations

ABSTRACT

Experimental testing is critical for evaluating the performance of novel structural systems. However, the cost of full-scale testing can be limiting. Small-scale testing provides a lower cost alternative that can produce reliable data if each component of the scaled model is properly developed. Given their stable hysteretic behavior, buckling-restrained braces (BRBs) are featured in several seismic force-resisting systems. The design of typical BRBs involves an axially yielding steel core that is prevented from buckling by a concrete casing. Designs for adaptable and easy-to-implement small-scale BRBs that can be included in structural testing have not been established. In this work, a small-scale BRB analog is developed that utilizes a core steel yielding plate that is prevented from buckling by a pair of steel casing plates. A flexural yielding mechanism is employed in the small-scale BRB analog, which allows for practical dimensions and the ability to independently tune brace stiffness and strength. Prototype braces were fabricated and validated through quasi-static cyclic testing in which they exhibited the full and stable hysteretic behavior characteristic of BRBs. To aid in the use of this BRB analog by others, numerical results were utilized to generate empirical equations that relate the strength and stiffness of the scaled BRB to the archetypical geometry of the core plate. Given its ability to deliver a stable hysteretic performance, the wide range of strength and stiffnesses that it can provide, and its easy reusability, the developed device is a good choice for experiments where a small-scale BRB analog is needed.

1. Introduction

Experimental testing is critical for evaluating the performance of novel structural systems. However, the cost of full-scale testing can be prohibitive or otherwise limiting to the range of investigation. Small-scale testing provides a lower cost alternative that can produce reliable data if each component of the scaled model is properly developed.

Choosing scaling ratios is an important component of the design of small-scale specimens, with different attributes, such as lengths, forces, and masses, necessarily scaled with different ratios to maintain similitude [1]. Due to the unique nature of each small-scale test of a structural system, as well as different laboratory capabilities, a wide range of scaling ratios have been utilized previously. Scaling ratios from a variety of small-scale experimental tests of structural systems on shake tables are listed in Table 1. Note that in each case, only three of the listed eight scaling ratios were chosen independently and the other five were necessarily derived from the chosen scaling ratios. As seen from these examples, the force scaling ratio is often much lower than the length scaling ratio. This result is natural as the force ratio is typically a dependent function related to the square of the independently chosen length ratio.

Given their stable hysteretic behavior, buckling-restrained braces (BRBs) are an important element of several seismic force-resisting systems including buckling restrained brace frames, strongback braced frames, and some outrigger systems. The most common type of BRB design consists of two main components – a steel core and a concrete filled steel tube casing. The steel core will extend out of the casing to form connections with other framing members. Tensile and compressive forces are resisted by the core and the casing acts as a restraining mechanism to prevent the core from buckling. A small gap is left between the steel core and the concrete fill and a debonding agent is applied to the surface of the steel core to decrease frictional interaction between the concrete fill and the steel core [8]. This minimizes the contribution of the casing to the overall axial strength. However, the compressive strength of BRBs is typically slightly higher than their tensile strength due to friction between the steel core and casing.

* Corresponding author at: 317 John D. Tickle Engineering Building, 851 Neyland Drive, Knoxville, TN 37996-2313, United States of America.
E-mail address: nwiersch@utk.edu (N.E. Wierschem).

https://doi.org/10.1016/j.jcsr.2023.107895
Received 31 December 2022; Received in revised form 27 February 2023; Accepted 6 March 2023
Available online 15 March 2023

While typical designs for BRBs use a concrete filled steel tube casing as a restraining mechanism, alternative designs are presented in the literature. This includes BRBs that follow the same basic design presented previously but with an all-steel casing rather than the typical concrete filled steel tube casing. The all-steel casing can be made from a combination of steel plates and HSS members [9,10], or may only use a specially fabricated steel plate [11].

Other forms of BRB exist, including those where the nonlinear response is not from axial yielding of a core. Attaching a "yielding brace system" connector to one end of a typical wide-flange brace produces a member that exhibits the desired hysteretic behavior [12,13]. This design concentrates plastic deformation in a series of yielding fingers that bolt into slotted holes at the end plate connection. The fingers bend during a seismic event and dissipate energy through flexural yielding.

While there are many different BRB designs, they all share a common design goal – stable, repeatable, symmetric hysteretic axial behavior. Fig. 1 shows the force-displacement results obtained from physical testing of a conventional brace and a BRB. The BRB exhibits mostly symmetric behavior without degradation in stiffness or strength. The conventional brace exhibits highly asymmetric behavior, i.e., the brace behaves differently in tension and compression, and notable strength and stiffness degradation.

Full-size BRBs have been thoroughly researched and have been widely implemented in practice. BRBs used in practice often have yield capacities that range from 350 to 10,000 kN [16]. Designs for self-described miniature BRBs have also been proposed [16,17]; however, the forces that these miniature BRBs are designed for, reported as low as 30 kN, are still much too large for them to be applicable for most scaled structural testing. Designs for adaptable and easy-to-implement small-scale BRBs that can be included in scaled structural testing have not been established. One of the main reasons for this are the very low force scales often present in scaled tests. It is difficult to produce BRBs that are simply highly scaled down versions of existing BRBs that are capable of precisely and accurately achieving the desired stiffness and strength. Furthermore, simply scaling down existing BRB designs would not be ideal in cases with multiple tests, as it would be advantageous for the BRBs to be quickly refurbished or replaced between tests.

In this work, a small-scale BRB analog is developed, which utilizes a core steel yielding plate that is sandwiched between and prevented from buckling by a pair of steel casing plates. Unlike most full-scale BRBs where the core yields axially, a flexural yielding mechanism is employed in the core plate of the small-scale BRB analog to allow more practical dimensions while maintaining the ability to independently tune the stiffness and strength of the brace. An archetype design for the core plate with parameterized geometry for this small-scale BRB analog was developed. Based on the archetype core plate design, a set of braces was fabricated and experimentally evaluated through quasi-static cyclic testing to examine their hysteretic behavior. To aid in the use of this BRB analog by others, the results from a numerical model of the archetype core plate design were utilized to generate empirical equations to relate the parameter values for the archetypal geometry of the core steel yielding plate with the strength and stiffness of the scaled BRB.

This paper is organized as follows. In Section 2, full-scale BRB stiffness and strength parameters considered are presented as well as scaled target values; furthermore, this section presents the design and modeling of the BRB analog developed in this work. In Section 3, experimental tests on the BRB analog and results are presented for several core plate configurations. Section 4 presents the development and evaluation of predictive equations to aid in the design of the BRB analog for future applications. Finally, the work is summarized and conclusions are presented in Section 5.

2. Design of BRB analog

This section discusses the design of the small-scale BRB analog device developed in this work. The main goal of the small-scale BRB analog is for it to exhibit a cyclic axial force-displacement response, including initial stiffness, yielding strength, and energy dissipation characteristics, that closely approximates that of a scaled prototype BRB. The resulting design must be applicable over a range of target strength and stiffness properties so that scaled prototype BRBs of differing core areas and lengths can be properly simulated. Additional details, including design drawings of the device, can be found in the second author's master's thesis [18].

2.1. Design parameters

The small-scale BRB analog was designed for future use in small-scale shake table tests which will employ a length scaling ratio of 1:12 (0.0833) and a force scaling ratio of 1:700 (0.00143). The resulting linear stiffness and modular scaling ratios are 1:58.3 (0.0172) and 1:4.86 (0.206), respectively. Based on previous work [19,20] and preliminary calculations, two target BRBs were identified and are designated as BRB-A and BRB-B. These represent traditional steel core BRBs that are roughly 5 m in length (work point to work point), have an expected core plate yield strength of 262 MPa, and core areas of 1935 mm^2 and 5806 mm^2, respectively. Values for the yield force, P_y, and initial elastic stiffness, K, for the target BRBs are listed in Table 2.

Despite the identification of these specific targets, the design of the small-scale BRB analog sought to accommodate a wider range of stiffness and strength parameters to ensure that the device would be useable in case of design changes and by other researchers. Furthermore, as strength and stiffness of a traditional BRB are both proportional to the cross-sectional area of the steel core, but, stiffness (and not strength) is inversely proportional to the length of the brace, independent control of both stiffness and strength was needed for the analog.

An additional design goal for the scaled BRB analog was to create a device that was as reusable as possible after it experiences inelasticity. This reusability is designed to help expedite and make more resource efficient scaled testing scenarios that include multiple tests where BRB inelasticity is anticipated.

2.2. Functionally similar, geometrically dissimilar model

Early in the design process, it was determined that a geometrically similar model would not be feasible. Given the scaling ratios, the cross-sectional area of the cores of BRB-A and BRB-B would need to be 13.4 and 40.3 mm^2 if the core was made of a material with appropriately scaled modulus and yield strength, which may be difficult to obtain. If steel with yield strength of 262 MPa were used, the core areas would

Table 1
Scaling ratios used in previous shake table tests.

Author & Year	Length ratio	Acceleration ratio	Modular ratio	Mass densit ratio	Stress ratio	Mass ratio	Force ratio	Time ratio
Chung et al. 1999 [2]	0.250*	1.00*	1.000	4.00	1.000*	0.0625	0.0625	0.500
Li et al. 2006 [4]	0.050*	1.16	0.177*	3.04*	0.177	0.0004	0.0004	0.207
Lu et al. 2008 [6]	0.500*	1.00*	1.000*	2.00	1.000	0.2500	0.2500	0.707
Lignos 2008 [5]	0.125*	1.00*	1.000*	8.00	1.000	0.0156	0.0156	0.354
Chunyu et al. 2012 [3]	0.025*	2.40	0.313*	5.20*	0.313	0.0001	0.0002	0.102
Lu et al. 2012 [7]	0.033*	2.50*	0.370	4.44	0.370*	0.0002	0.0004	0.115

* Ratios with asterisk are independently chosen. All other ratios are dependently calculated.

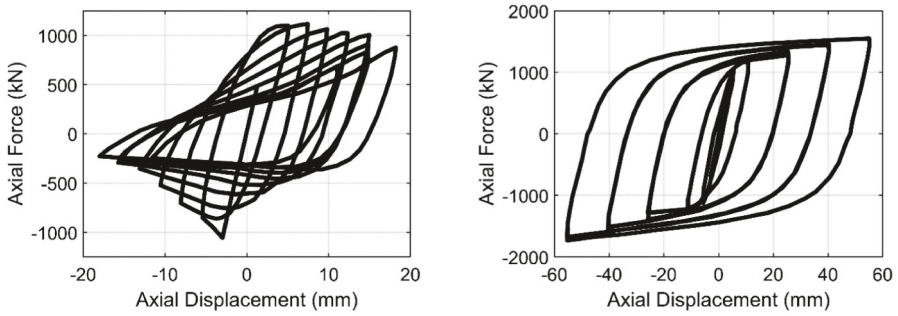

(a) Conventional brace (Specimen "Strut 19", reproduced from [14])

(b) Buckling restrained brace ("Specimen 1", reproduced from [15])

Fig. 1. Example hysteretic force-displacement response for conventional and buckling restrained braces [14,15].

Table 2
Yield force and elastic stiffness values for prototype and model BRBs.

BRB designation	Full-scale model values			Scaled target values	
	Core area (mm^2)	K (N/mm)	P_y (N)	K (N/mm)	P_y (N)
BRB-A	1935	116,000	507,000	1990	725
BRB-B	5806	348,000	1,521,000	5974	2175

need to be 2.8 and 8.3 mm^2 to achieve an appropriately scaled yield force. Fabrication of axially yielding components this size within tolerance would pose a significant challenge.

In this work, the force-displacement behavior of the BRB analog is important, not its material stress-strain behavior. Consequently, a geometrically dissimilar model is acceptable as long as the overall scaled force-displacement behavior of the device is accurate. The two-step process used to arrive at a functionally similar, but geometrically dissimilar scaled model is seen schematically in Fig. 2. The strength of this two-step process is that it frees the designer from many geometric and material constraints and leaves only the functionality constraint (i.e., delivering the scaled force-displacement behavior of the BRB).

2.3. Device design

The design for the BRB analog is shown in Figs. 3 and 4. This design follows the two-step process outlined in Fig. 2 by achieving scaled elastic stiffness and yield strength goals (identified in Step #1) without being constrained to the scaled-down geometry and mechanism of the prototype (Step #2). The BRB analog consists of an internal core plate, detailed in Fig. 3, and casing plates that restrain the out-of-plane buckling of the core plate. The core plate extends beyond the casing plates to make connections with the structural system, or in the case of this work, with the grips of a universal testing machine. One restraining bolt passes through holes in the two casing plates and the core plate to hold the casing plates in place. Three additional alignment bolts pass through holes in the two casing plates and slots in the core plate maintain alignment of the casing plates and restrain in-plane buckling of the core plate. The restraining bolt and alignment bolts are installed finger tight to limit the effect of friction between the core plate and the casing plates. Other bolts connecting the BRB analog to the structural system or machine grips are tightened to prevent slip that would affect the force-displacement relationship.

Axial load in the BRB analog results in bending of components of the core plate that are oriented perpendicular to the load, these are referred to as bending links (see Fig. 3). The stiffness and strength of these bending links controls the overall axial force-displacement relationship of the BRB analog. The rest of the core plate was designed to remain elastic. While the design produced in this study is unique, inspiration for the use of a flexural mechanism was drawn from several all-steel prototype BRBs presented in the introduction, most notably those examined by Gray et al. [12,13].

The relative simplicity of the core plate design makes the yield force and elastic stiffness of the BRB analog relatively predictable and controllable. Specifically, the dimensions w, b, and L in Fig. 3 can be varied to tune the behavior of the BRB analog and allow the same basic plate design to provide a wide range of strengths and stiffnesses. By assuming all of the compliance in the BRB core plate is in the bending links, treating each of the four bending links as a fixed-end beam, and combining standard relationships for the deformation and moment capacity of fixed-end beams, the axial stiffness and strength of the BRB analog can be approximated as

$$K = \frac{8Etb^3}{L_{eff}^3} \tag{1}$$

$$P_y = \frac{2F_y tb^2}{L_{eff}} \tag{2}$$

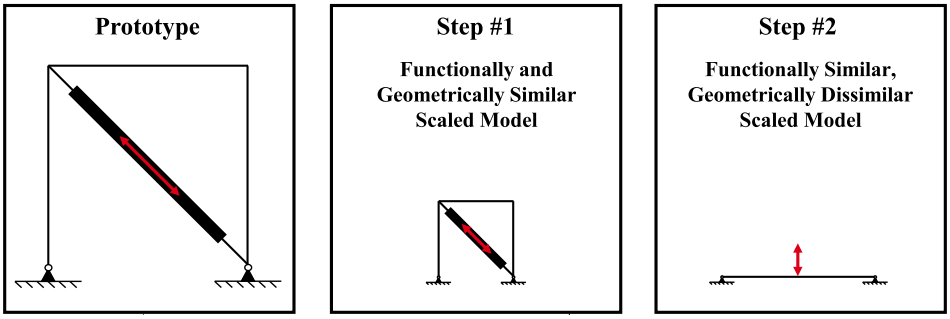

Fig. 2. Schematic two-step similitude process for geometrically dissimilar scaled models.

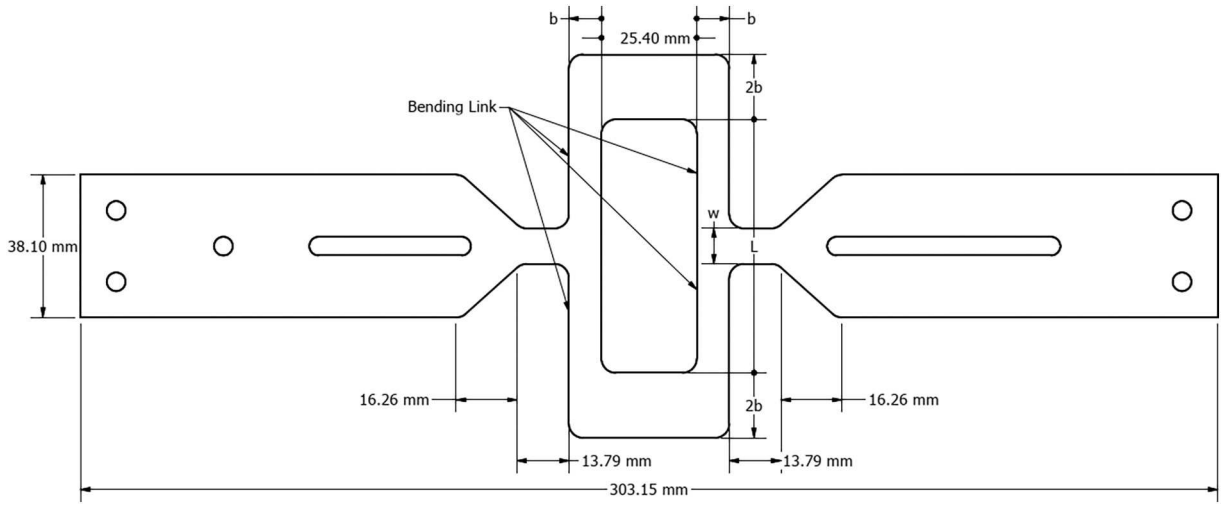

Fig. 3. Device core plate labeled with important design parameters (thickness, $t = 3.04$ mm).

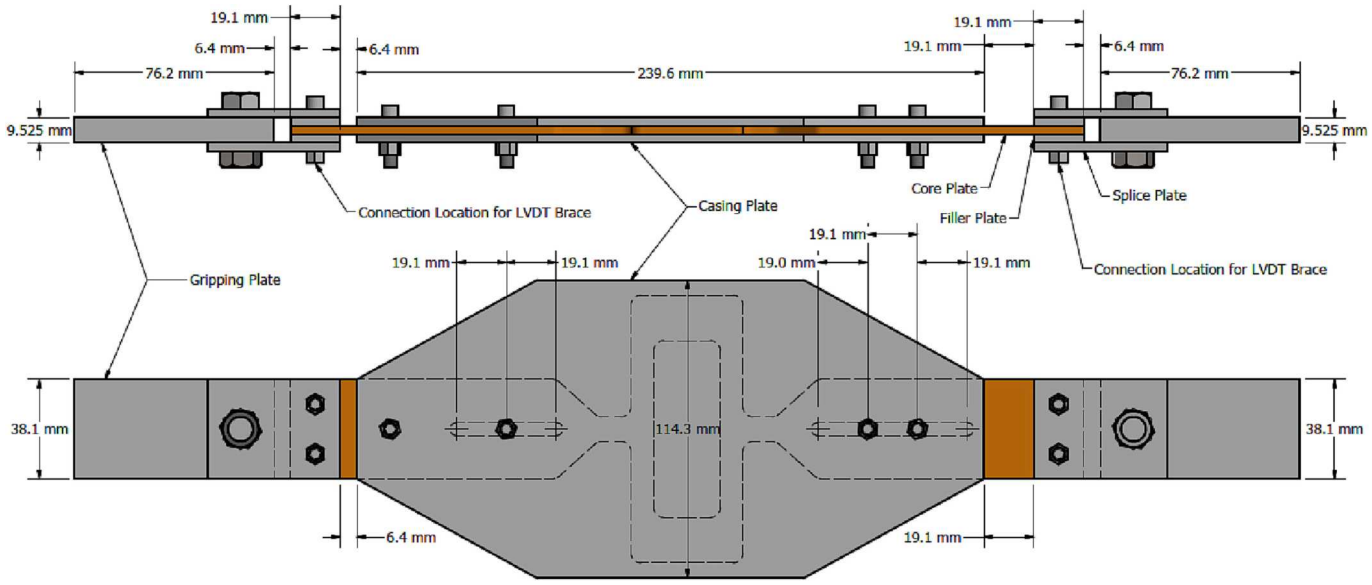

Fig. 4. Assembled test mechanism for small-scale BRB. LVDT and LVDT braces not shown.

where, K is the axial stiffness of the BRB analog, P_y is the yield force of the BRB analog, t is the core plate thickness, b is the width of the bending links, and $L_{eff} = L - w$ (w, b, and L are shown in Fig. 3).

Eqs. (1) and (2) can aid in the initial design of the brace as they can be used to compute approximate values for dimensions w, b, and L that provide target stiffness and strength. More refined values can be obtained from numerical analyses as described in the following subsection or through the empirical equations developed in Section 4.

The all-steel, all-bolted construction of the BRB analog allows for relatively simple fabrication and replacement of the core plate between tests in a series. The casing plates and bolts do not experience significant loads and can be reused many times in experimental testing.

2.4. Numerical modeling

Finite element modeling of the core plate enables more precise design of the dimensions of the core plate. Given the configuration of the BRB analog and assuming that 1) the casing plates fully restrain out-of-plane buckling of the core plate and 2) friction between the core plate and other components is negligible, a two-dimensional plane stress analysis of the core plate only is sufficient to predict the force-displacement response of the BRB analog. Accordingly, neither the casing plates nor contact from the casing plates are included in the numerical model. In this work, the finite element analysis software Abaqus/CAE (Version 6.12) was used to perform the analyses.

Linear plane stress quadrilateral elements with reduced integration (CPS4R) were used to mesh the core plate. Based on the results of a mesh refinement study, 8 elements were used across the width of the bending links. The central portion of the core plate was meshed with elements approximately the same size as those in the bending links. The remainder of the core plate was meshed with elements approximately twice the size as those in the bending links. The finite element mesh for BRB-B is shown in Fig. 5. Consideration of nonlinear geometry effects was enabled in the model to account for the impact of large strains or large deformations in the analysis.

To simplify the analyses, the loads and boundary conditions were not placed at the bolt holes near the ends of the core plate where the core plate was connected in reality; rather, loads and boundary conditions were placed at the ends of the plate. Longitudinal and transverse displacements were restrained along one end (i.e., the left end in Fig. 5) and

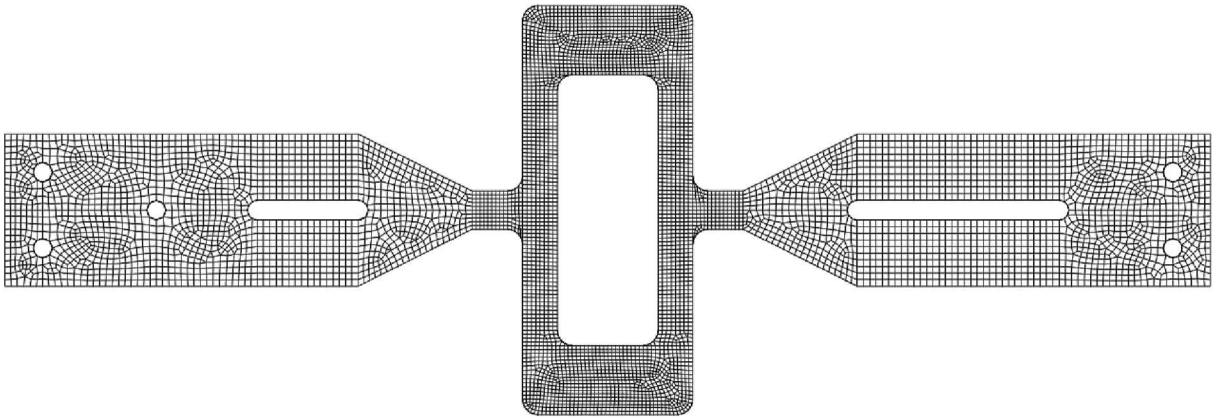

Fig. 5. Two-dimensional finite element mesh of the core plate for BRB-B.

load in the longitudinal direction was applied on the other end by specifying displacements. The restraint provided by the alignment bolts was represented in the model by restraining transverse displacements at discrete points along the slotted holes.

A Chaboche model with nonlinear isotropic hardening was used for the constitutive relation of the core plate. This model was input in Abaqus using the "combined" hardening type with 3 backstresses and true stress-true plastic strain data listed in Table 3 derived from the coupon tests described in Section 0. Cyclic hardening parameters were defined based on the coupon tests and recommendations from the literature [21,22]. These parameters include the equivalent stress at which hardening begins ($\sigma_{y0} = 235.8$ MPa), the maximum radius of the yield surface ($Q_\infty = 60.3$ MPa), and the exponential material hardening parameter ($b = 17.58$).

As an illustration of the behavior of the BRB analog, Fig. 6 shows the deflected shape and stresses in the core plate of BRB-B near the onset of yielding. These results confirm that flexure in the bending links dominates the response of the BRB analog.

3. Experimental tests

Quasi-static cyclic experimental tests were performed to confirm the performance of the BRB analog. Casing plates and three core plates were fabricated. Each of these pieces was water jet cut from 11-gauge ASTM A1011-CS-B steel. The measured thickness of this material used for the casing plates and core plates was $t = 3.04$ mm. Additionally, coupons were cut from the steel to determine material properties in accordance with ASTM E8 [23]. Based on the average of three coupon tests, the yield strength of the material was $F_y = 237$ MPa, the tensile strength of the material was 342 MPa, and the elongation was 40% for a gage of 50.8 mm.

Values of w, b, and L (Fig. 3) were selected using the finite element model described in Section 2.4 to achieve the target stiffness and yield strengths listed in Table 2. The predicted performance metrics and core plate geometric parameters for the BRBs are shown in Table 4. The predicted values that were determined from the results of numerical simulations for strength and stiffness for the BRB analogs shown in this table match well with the scaled target values shown in Table 2.

Table 3
Stress-strain data used to define the constitutive relation in the finite element model.

True stress (MPa)	True plastic strain
235.8	0.0000
249.6	0.0193
310.2	0.0546
356.4	0.1002

For these BRBs, the same material was used for the core plate and casing plates. Use of the same thickness was determined to be adequate to restrain out-of-plane buckling of the core plate and other potential buckling modes (e.g., overall buckling and global buckling) and was convenient for fabrication. The same thickness may not be adequate in other cases and the stability of the BRB analog should be carefully considered in future designs based on the specific design and the structure to which the BRB is attached. In some cases, thicker casing plates or additional stiffeners may be needed to avoid stability issues, such as out-of-plane buckling.

3.1. Experimental methods

Experimental testing of the BRB analog with the two different core plates was done using an MTS 858 Table Top System with a load capacity of 25 kN. Hydraulic wedge grips with a serrated surface were used to hold the specimen for these tests at gripping plates which were bolted to the core plate as shown in Fig. 7. The applied load was recorded using the machine's internal load cell. Axial displacement was measured using a LVDT attached to fixtures bolted to the ends of the core plate.

The loading protocol used for the experimental testing was a slightly modified version of the loading protocol required for qualification testing of buckling-restrained braces provided in Section K3 of the American Institute of Steel Construction (AISC) Seismic Provisions for Structural Steel Buildings [24]. The protocol is based on the expected axial displacement at brace yield (Δ_{by}) and the expected axial displacement at the design story drift (Δ_{bm}). Two cycles of loading at seven different levels of displacement (i.e., $0.5\Delta_{by}$, $1.0\Delta_{by}$, $0.5\Delta_{bm}$, $1.0\Delta_{bm}$, $1.5\Delta_{bm}$, $2.0\Delta_{bm}$, and $3.1\Delta_{bm}$) were performed. The initial cycles at $0.5\Delta_{by}$ displacement are not included in the standard loading protocol, but were included to ensure that the elastic response of the BRB was well-captured. The final cycles at $3.1\Delta_{bm}$ displacement are also not included in the standard loading protocol, but were included to evaluate the behavior of the BRB analog at very high levels of scaled displacement demand. The standard loading protocol requires additional cycles of loading at $1.5\Delta_{bm}$ displacement until the brace achieves a cumulative inelastic axial deformation of at least 200 times the yield deformation. However, it was determined that there was no need for additional cycles because each brace tested had already reached a cumulative inelastic deformation of over 200 times the yield deformation by the end of the cycles at $2.0\Delta_{bm}$ displacement.

The axial displacement at brace yield, Δ_{by}, was estimated using the finite element model of the brace, $\Delta_{by} = 0.36$ mm for both braces. The AISC Seismic Provisions [24] places a lower limit of 1% of the story height on the expected brace axial displacement at the design story drift, Δ_{bm}. Given that the BRB analog is being generally designed, the design story drift is unknown; therefore, the minimum was used and approximated as $\Delta_{bm} = 3.3$ mm.

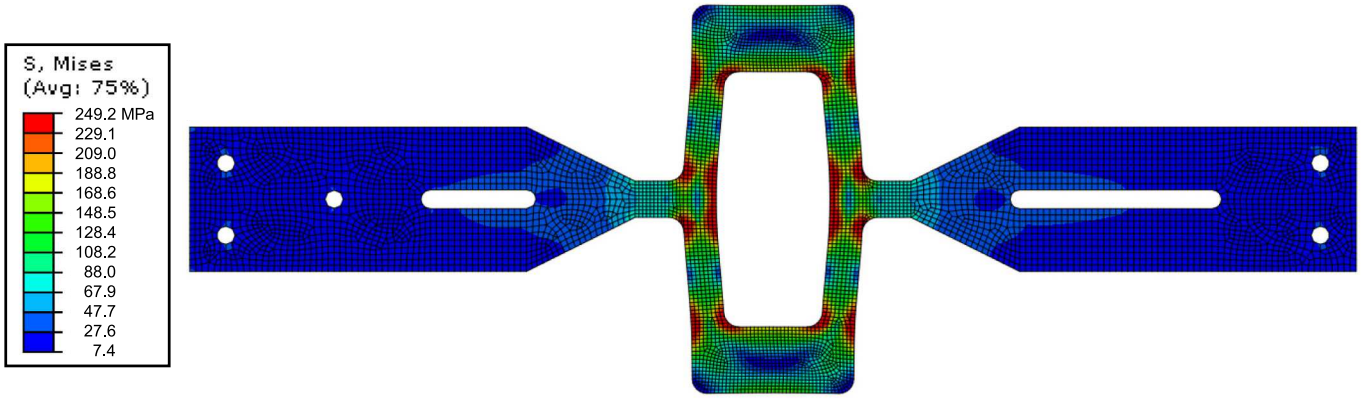

Fig. 6. Finite element analysis results of the core plate for BRB-B. Analysis results at displacement of 0.5 mm. Von Mises stress shown on the deflected shape (scale factor = 10).

Table 4
BRB analog core plate dimensions, predicted performance values, and experimental performance values.

	Core plate dimensions			Values predicted from numerical simulations		Values from experiments	
BRB designation	L (mm)	b (mm)	w (mm)	K (N/mm)	P_y (N)	K (N/mm)	P_y (N)
BRB-A	58.29	4.34	9.53	2002	734	1925	703
BRB-B	67.84	8.69	9.53	5979	2202	5932	2193

A maximum loading rate of 1.2 mm/min was used for the initial four cycles (with target displacements of $0.5\Delta_{by}$ and $1.0\Delta_{by}$). A maximum loading rate of 4.8 mm/min was used for the next four cycles (with target displacements of $0.5\Delta_{bm}$ and $1.0\Delta_{bm}$). A maximum loading rate of 9.6 mm/min was used for the remaining six cycles (with target displacements of $1.5\Delta_{bm}$, $2.0\Delta_{bm}$, and $3.1\Delta_{bm}$). The total time for the test was approximately 45 min. A plot of the imposed displacement vs time for BRB-A is shown in Fig. 8.

3.2. Experimental results

The experimental force-displacement curves of the BRB analogs are shown in Fig. 9. These curves were plotted using the force measured from the machine's load cell and the displacement measured from the LVDT attached directly to the ends of the core plate. Both curves exhibit the full stable hysteretic behavior characteristic of BRBs.

Figs. 10 and 11 show the initial elastic cycles and the first excursion beyond yield for BRB-A and BRB-B, respectively. The BRB analogs were in tension for the first excursion beyond yield. The initial elastic stiffness and yield force were calculated from the data in Figs. 10 and 11. The initial elastic stiffness was calculated as the average slope of the tensile and compressive regions from the initial elastic cycles. The yield force was determined as the ordinate of the intersection point between a line following the initial elastic slope and a line following the initial plastic slope. The two lines are shown as dashed lines and their intersection is shown as a dot in Figs. 10 and 11.

The accuracy of the finite element model presented in Section 2.4 to predict the elastic stiffness and yield force of the BRB analog is confirmed through comparison of experimental and numerical results. Figs. 10 and 11 also show the force-displacement response from the numerical simulation of the BRB analogs. The initial elastic stiffness and yield point were identified from the numerical results in the same manner as for the experimental results.

Fig. 7. Setup used for experimental axial testing of BRB analog. BRB analog is being held in loading frame with hydraulic grips. LVDT is not attached.

The values of initial elastic stiffness and yield force calculated from the numerical and experimental results for both BRB analogs are listed in Table 4. The good comparison of these values shown in Table 4 along with the similar behavior shown in Figs. 10 and 12 demonstrates that the finite element model matches the initial experimental behavior well and provides a close estimate of the response parameters. With this close match over a relatively wide range (i.e., the strength and stiffness of BRB-B are 208% and 209% larger than for BRB-A, respectively), there is

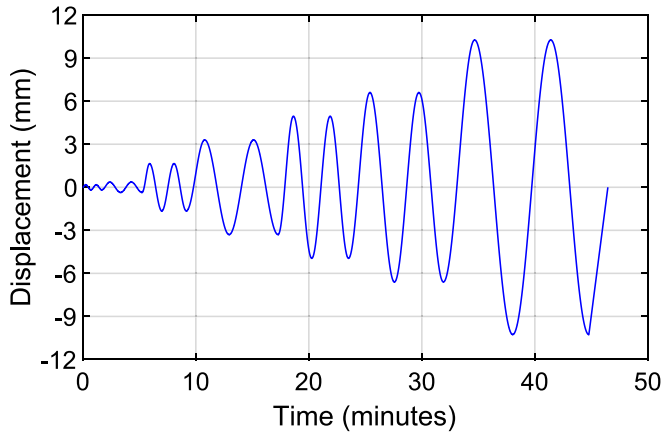

Fig. 8. Example imposed brace displacement for the adopted testing protocol.

confidence that the finite element model can be used to accurately estimate the response parameters with other values for the core plate geometric parameters.

3.3. Alternative Core plate design

The development of the BRB analog focused on rectangular core plates as they were best able to mimic the force-displacement relationship of full-scale BRBs. However, the BRB analog can accommodate other core plate designs. While limited to planar geometry, the design of the device in this work allows for a large design space, with the potential for other designs to produce significantly different behavior (e.g., significant post-yield stiffness, asymmetry between tension and compression, and cyclic degradation). This different behavior increases the use cases for this device as it could be utilized as an experimental analog for devices with behavior that is significantly different than traditional BRBs, such as conventional braces and other yielding dampers.

An example of an alternative core plate design is shown in Fig. 12. Instead of a central rectangle where yielding is concentrated, this design features a central circular zone. As indicated in the figure, this design is also parameterized by several features of the geometry: the circle's outer diameter (A), the circle's inner diameter (B), and the length of one of the plate's transition zones (C). These parameters allow for the alteration of the resulting brace performance attributes.

An example of the force-displacement relationship for a brace with a circular core plate is shown in Fig. 13. This force-displacement relationship was experimentally measured from a test performed as described earlier in this section and utilizes the same plate material for the rectangular core plates. The parameter values of the circular core plate used for this test are A = 49.78 mm, B = 42.44 mm, and C = 25.10 mm. Instead of the full and symmetric hysteretic behavior that is seen from the braces with a rectangular core plate, the force-displacement relationship with this circular core plate is noticeably asymmetric with significant hardening in tension. The reason for this asymmetry lies in the core plate geometry. At large tensile displacements the circle straightens out and stiffens. However, under large compressive displacements, the circle squashes and softens.

The alternative core plate geometry shown in Fig. 12 and resulting force-displacement relationship shown in Fig. 13 is just one example. If desired, different core plate designs can be used to replicate a range of different hysteretic behaviors. Depending on the complexity of the geometry and desired response parameters, numerical simulations in combination with optimization techniques might be employed in the specialized design of these core plates. Numerical simulations of the

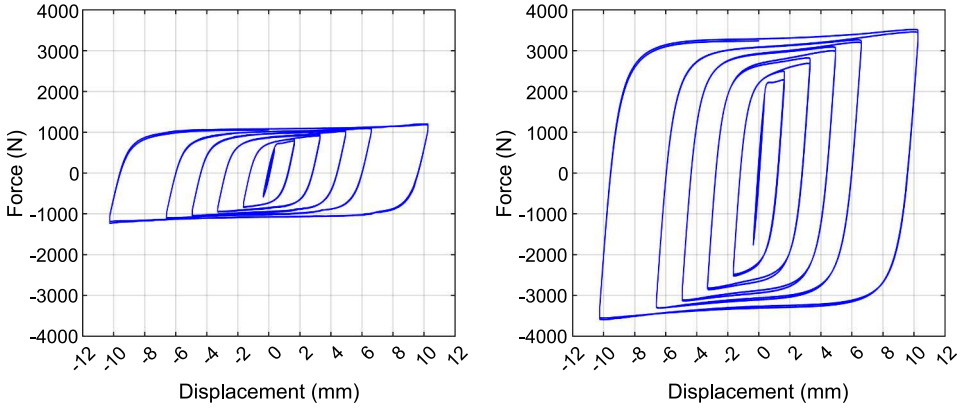

Fig. 9. Comparison of BRB-A (left) and BRB-B (right) experimental force-displacement hysteretic curves.

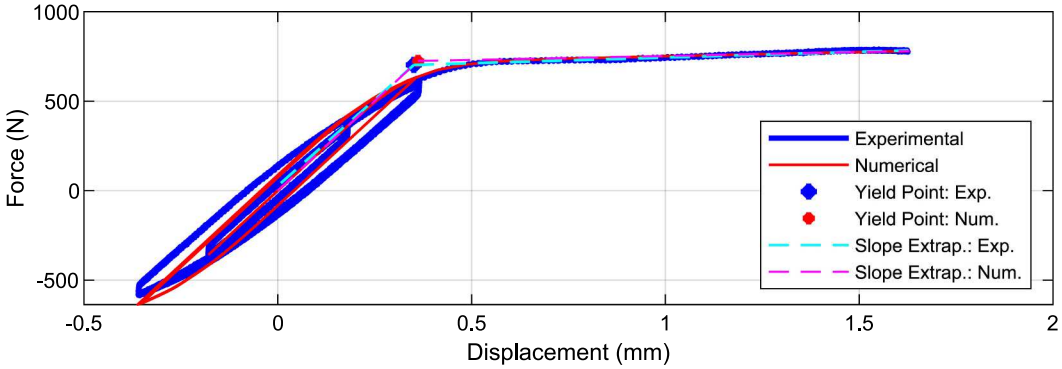

Fig. 10. Graphical comparison of experimental and numerical initial cyclic behavior for BRB-A.

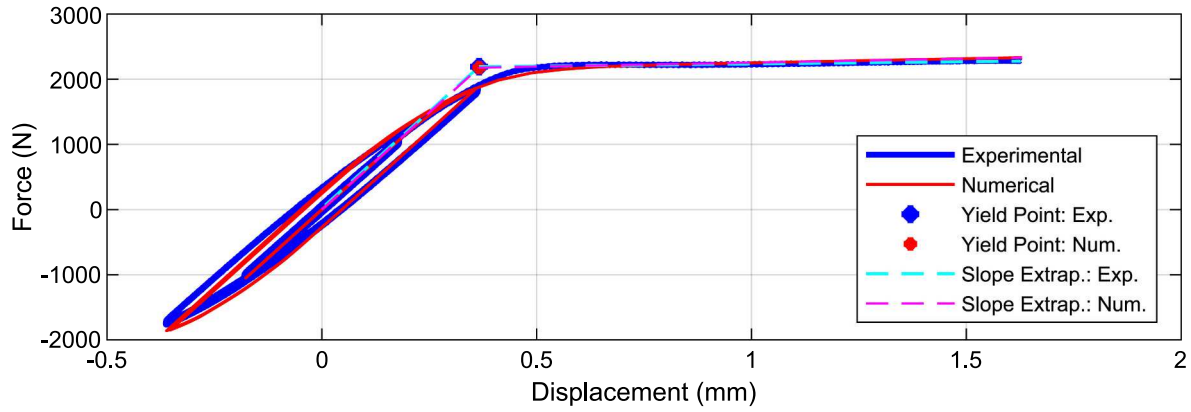

Fig. 11. Graphical comparison of experimental and numerical initial cyclic behavior for BRB-B.

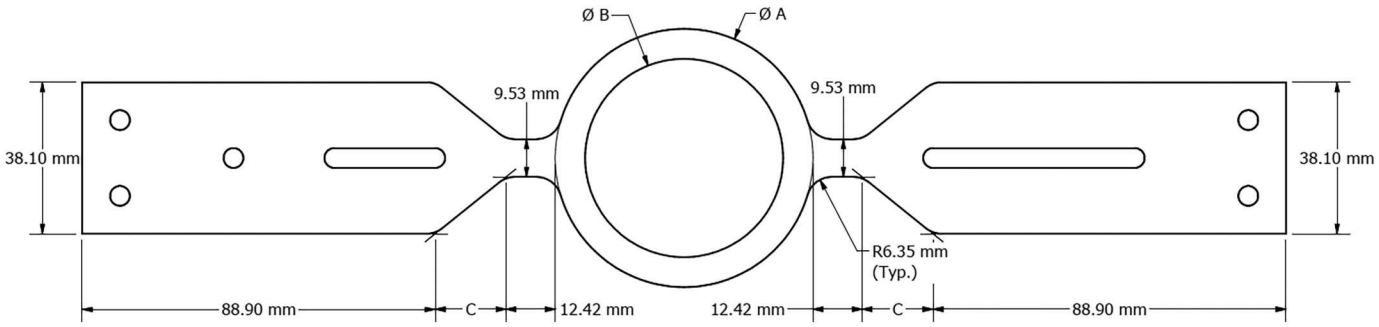

Fig. 12. Design for a circular core plate, an example alternative core plate geometry.

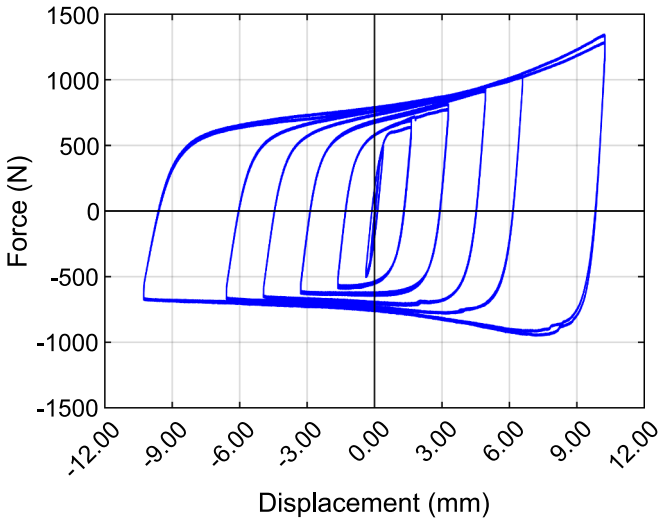

Fig. 13. Example hysteretic curve resulting from a scaled brace with a circular core plate.

behavior resulting with different core-plate geometry could be undertaken with the same modeling approach as described in Section 2.4.

4. Development and evaluation of empirical equations

The initial elastic stiffness, K, and yield force, P_y, of the BRB analog can be approximated using Eqs. (1) and (2). These equations were developed assuming the only deformation of the core plate was in the bending links and that the bending links acted as fixed-end beams. More accurate predictions of K and P_y can be obtained from numerical simulations which consider the deformations of all components of the core plate and not just flexural deformation of the bending links. This section describes the development of equations for K and P_y that can be used in lieu of numerical analyses but that are similarly accurate. Such equations are useful for designing the dimensions of the core plate to achieve specific values of K and P_y.

The equations are calibrated to the results of numerical simulations using the finite element model and thus are empirical in nature; however, the format of the equations is based on Eqs. (1) and (2), which are mechanistic. Several correction factors and coefficients were added to Eqs. (1) and (2) to form the basis of the empirical equations shown in Eqs. (3) and (4). These correction factors and coefficients are designed to account for difficult to calculate variations in the operative length and width of the bending links due to the core plate geometry, deviations from the assumed bending link boundary conditions, and differences due to the compliance of the core plate outside the bending links. The exact form of the correction factors and coefficients in Eqs. (3) and (4) was determined in part using trial and error.

$$K = [C_1 + C_2\alpha(1-\lambda)]\frac{Et[(1+C_3\beta)b]^3}{[(1+C_4\beta)L_{eff}]^3} \tag{3}$$

$$P_y = [C_5 + C_6\alpha(1-\lambda)]\frac{F_y t[(1+C_7\beta)b]^2}{(1+C_8\beta)L_{eff}} \tag{4}$$

where, $\alpha = w/L$, $\beta = b/L_{eff}$, $\lambda = (w_0\text{-}w)/L$, $w_0 = 9.53$ mm, and C_1 through C_8 are dimensionless constants that are quantified using a regression analysis.

A series of numerical analyses using the finite element model described in Section 2.4 were performed with different values of w, b, and L to quantify the constants in Eqs. (3) and (4). The initial elastic stiffness, K, and yield force, P_y, were determined from each analysis. The combined sets of input and output values were used as training data in a

regression analysis. Table 5 lists the core plate geometric parameters and resulting response measures calculated from the numerical simulation results for three data sets: training data set, in-bounds data set, and out-of-bounds data set. For each of these data sets, the plate thickness was 3.04 mm and the material properties introduced in Section 2.4 were used.

The training data set is used to fit the empirical equations and determine the calibration constants in the equations; thus, this training data should include enough parameter combinations and diverse enough parameter combinations such that the behavior of the device over a range of elastic stiffnesses and yield forces can be thoroughly investigated. However, it was also important that this training data did not include outliers representing a combination of parameters unlikely to be used in the BRB analog, as the inclusion of such outliers might ultimately reduce the accuracy of the equations for the more likely parameter combinations. For this training data set, the lower and upper bounds of the length parameter (L) were set to 50.80 and 76.20 mm, respectively. The lower and upper bounds for the width parameter (b) were set to 96.77 and 290.32 mm, respectively. All of the parameter combinations in the training data set have $w = 9.53$ mm, which was the value of w used for both experimental tests. A list of all 24 training data points is presented in Table 5. As seen in this table, the elastic stiffness of the resulting training data set spans from 1576 to 11,092 N/mm and the yield force spans from 494 to 3888 N; thus, this training data set covers a wide range of potential BRB analogs.

The "in-bounds" data set in Table 5 is described as in-bounds because all values of L and b are chosen such that they do not extend past either the lower or upper bound of the training data. However, values of w other than the original connecting width of 9.53 mm are tested. None of these lengths or widths were previously used in the training data, and the values of all three parameters under consideration (L, b, and w) are within a reasonable range of the training data, so it is expected that the empirical equation fit with the training data set will predict well the elastic stiffness and yield force for the 8 combinations in this data set.

The accuracy of the empirical equations at predicting the elastic stiffness and yield force of BRB analogs with core plate geometric parameters outside of what is used for the training data set is of interest. To explore this, six data points were included in an "out-of-bounds" data set that is also shown in Table 5. For each point in this data set, one or both of the parameters L or b is beyond the limits of the values used in the training data set. A limit of 15% deviation from the original bounds was set as the maximum, so that these geometric parameters are still reasonable. Table 4 shows the geometric parameters chosen, as well as the calculated values of the response measures from the numerical simulations. As this out of bounds data set includes geometric parameters beyond what is used for the training, it is expected that the predictive empirical equations will be less effective, but it is unclear how effective the empirical equations will be for these cases.

The relationship between elastic stiffness and yield force from the numerical simulation results is shown in Fig. 14. This figure shows that the elastic stiffness and yield force for the BRB analogs simulated have some scatter, but that their elastic stiffness and yield force values are largely proportional. This proportionality is similar to what is anticipated in the design of traditional BRBs. Furthermore, this graph shows that in-bounds and out-of-bounds training sets have elastic stiffness and yield force combinations that are similar to the space covered by the training data set.

With the geometric parameters and response measures from the training set, the constants of the empirical equations were solved for using a nonlinear regression analysis. The empirical equations with the resulting constants are shown in Eqs. (5) and (6).

$$K = [11.030 - 2.579\alpha(1-\lambda)]\frac{Et[(1-0.487\beta)b]^3}{[(1+2.561\beta)L_{eff}]^3} \tag{5}$$

$$P_y = [2.011 + 6.432\alpha(1-\lambda)]\frac{F_y t[(1-0.847\beta)b]^2}{(1-0.847\beta)L_{eff}} \tag{6}$$

Table 5
Training, in-bound, and out of bound data sets used to calibrate and evaluate empirical equations. Data set includes core plate geometric parameters and response measures determine from numerical simulation results.

Test #	L (mm)	b (mm)	w (mm)	K (N/mm)	P_y (N)
Training Data Set					
T1	50.80	3.81	9.53	2220	707
T2	50.80	5.08	9.53	4067	1205
T3	50.80	6.35	9.53	6267	1810
T4	57.15	3.81	9.53	1576	578
T5	57.15	5.08	9.53	2991	1005
T6	57.15	6.35	9.53	4758	1526
T7	57.15	7.62	9.53	8901	2825
T8	63.50	3.81	9.53	1153	494
T9	63.50	5.08	9.53	2249	859
T10	63.50	6.35	9.53	3669	1312
T11	63.50	7.62	9.53	5336	1850
T12	63.50	8.89	9.53	7181	2460
T13	63.50	10.16	9.53	9123	3149
T14	63.50	11.43	9.53	11,092	3888
T15	69.85	6.35	9.53	2870	1148
T16	69.85	7.62	9.53	4253	1628
T17	69.85	8.89	9.53	5831	2180
T18	69.85	10.16	9.53	7539	2793
T19	69.85	11.43	9.53	9313	3470
T20	76.20	6.35	9.53	2278	1019
T21	76.20	7.62	9.53	3434	1450
T22	76.20	8.89	9.53	4777	1944
T23	76.20	10.16	9.53	6265	2509
T24	76.20	11.43	9.53	7847	3123
In-bounds Data Set					
In1	53.34	4.45	8.00	2528	832
In2	55.88	5.72	8.38	3881	1263
In3	58.42	5.72	8.76	3524	1192
In4	60.96	6.99	9.14	4877	1650
In5	66.04	8.26	9.91	5782	2055
In6	68.58	9.53	10.29	7079	2576
In7	71.12	9.53	10.67	6604	2473
In8	73.66	10.80	11.05	7834	3011
Out-of-bounds Data Set					
Out1	50.80	3.25	9.53	1544	516
Out2	43.18	3.81	9.53	3498	921
Out3	43.18	3.25	9.53	2505	685
Out4	76.20	13.16	9.53	10,054	4030
Out5	87.63	11.43	9.53	5832	2638
Out6	87.63	13.16	9.53	7671	3430

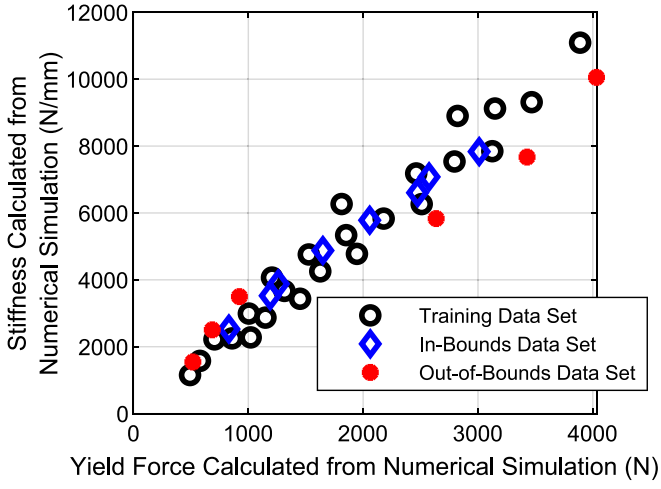

Fig. 14. Elastic stiffness vs yield force from numerical simulation results.

Figs. 15 and 16 show the error between the elastic stiffness and yield force calculated from the numerical simulations and predicted from the empirical equations in Eqs. (5) and (6), respectively. Most data points are estimated with the empirical equations within ±2% of the calculated value from the numerical simulation; however, there are exceptions. The most obvious of these exceptions are the three data points in the out-of-bounds test data set that utilize lengths and widths below the lower limit of the training set. The error in the predicted elastic stiffness and yield force is approximately 4–8%. This is high when considering most other predictions are below 2% error. This shows that the predictive capability of the empirical equations breaks down if extrapolating past the lower bound of either geometric parameter. While this is not ideal, it is not an area of concern because the low level of elastic stiffness and yield force of the BRB analogs present in these cases appear to be achievable with a combination of geometric parameters covered by the parameter ranges the empirical equations were trained with.

In addition to this, it is noticeable that there is a poorer fit to the data for lower elastic stiffness and yield force in general. But, these low stiffness values and higher estimation error generally correspond to a width of $b = 3.81$ mm or less. These small widths are at the lower bound of practical values, so the larger error here is considered acceptable. In contrast, the data points past the upper bounds of the training data limits appear to be well estimated. These results provide confidence that the final form of the predictive equations will be highly useful in determining required dimensions for model BRBs based on the values of scaled strength and stiffness requirements even if the necessary strength and stiffness values are higher than currently expected and require a larger geometry.

5. Conclusions

The objective of this work was to develop a small-scale analog that closely mimics the force-displacement response of buckling restrained braces (BRBs) for use in scaled physical experiments of structural systems. The scaled BRB analog designed in this work uses a central core steel yielding plate that is prevented from buckling by a pair of casing plates. The central core plate resists the axial tension and compression of the BRB analog through in-plane bending and can be designed to provide different hysteretic properties. The focus of this work was on a rectangular core plate design. Key observations and conclusions from the development of this BRB analog are:

- The BRB analog exhibits a full and nearly symmetric force-displacement curve that resembles that of full-scale BRBs.
- A relatively simple two-dimensional plane stress finite element analysis model of the core plate accurately captures the elastic stiffness and yield force of the BRB analog and can be used to design the core plate dimensions.
- Empirical equations developed based on results from the finite element analysis model accurately capture the elastic stiffness and yield force of the BRB analog (with typically less than 2% error and less than 8% error for all cases examined in comparison to results from the finite element analysis) and can also be used to design the core plate dimensions.
- Consisting of only steel plate material and bolted connections, the BRB analog is relatively simple to fabricate and accommodates replacement of the core plate (i.e., reuse of the casing plates) for repeated testing.

Thus, the BRB analog developed in this work is an effective and practical option to represent BRBs in a range of scaled experiments of structural systems. The availability of this device will enhance future research advancing the understanding of structural system behavior.

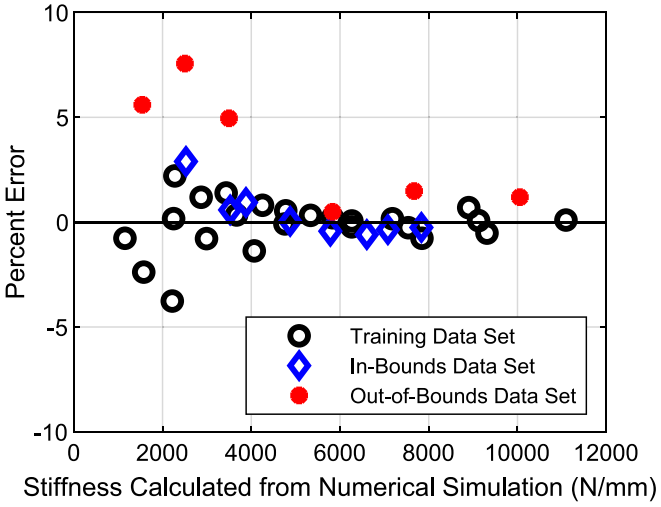

Fig. 15. Error in fit from elastic stiffness empirical equation.

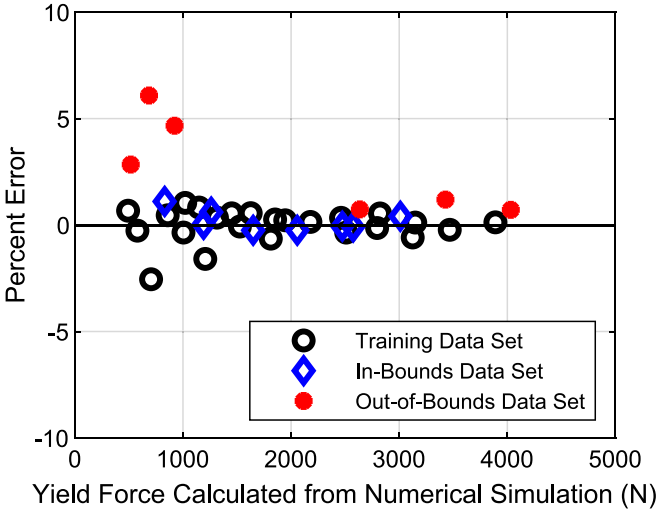

Fig. 16. Error in fit from yield force empirical equation.

CRediT authorship contribution statement

Nicholas E. Wierschem: Conceptualization, Writing – original draft, Visualization, Supervision, Funding acquisition. **Lindsay Kirk:** Methodology, Formal analysis, Investigation, Writing – original draft, Visualization. **Mark D. Denavit:** Conceptualization, Writing – review & editing, Project administration, Funding acquisition.

Declaration of Competing Interest

The authors declare that they have no known competing financial interests or personal relationships that could have appeared to influence the work reported in this paper.

The authors declare the following financial interests/personal relationships which may be considered as potential competing interests:

Mark Denavit reports financial support was provided by National Science Foundation. Nicholas Wierschem reports financial support was provided by National Science Foundation.

Data availability

Data will be made available on request.

Acknowledgements

The authors would like to acknowledge the support of Zach Arwood during the experimental testing of the BRB analog and Andy Baker and Larry Roberts for the fabrication of the BRB analog.

This work was supported by the National Science Foundation under Grant No. 1940197. Any opinions, findings, and conclusions or recommendations expressed in this material are those of the authors and do not necessarily reflect the views of the National Science Foundation.

References

[1] E. Buckingham, On physically similar systems; illustrations of the use of dimensional equations, Phys. Rev. 4 (4) (1914) 345–376, https://doi.org/10.1103/PhysRev.4.345.
[2] W.J. Chung, C.B. Yun, N.S. Kim, J.W. Seo, Shaking table and pseudodynamic tests for the evaluation of the seismic performance of base-isolated structures, Eng. Struct. 21 (4) (1999) 365–379, https://doi.org/10.1016/S0141-0296(97)00211-3.
[3] T. Chunyu, X. Congzhen, Z. Hong, C. Jinzhe, Shaking table test and seismic performance evaluation of Shanghai tower, Int. J. High-Rise Build. 1 (3) (2012) 221–228.
[4] C.S. Li, S.S. Lam, M.Z. Zhang, Y.L. Wong, Shaking table test of a 1:20 scale high-rise building with a transfer plate system, J. Struct. Eng. 132 (11) (2006) 1732–1744, https://doi.org/10.1061/(ASCE)0733-9445(2006)132:11(1732).
[5] D.G. Lignos, H. Krawinkler, Sidesway Collapse of Deteriorating Structural Systems under Seismic Excitations, Stanford University, 2012.
[6] X. Lu, G. Fu, W. Shi, W. Lu, Shake table model testing and its application, Struct. Design Tall Spec. Build. 17 (1) (2008) 181–201, https://doi.org/10.1002/tal.338.
[7] X. Lu, Y. Chen, Y. Mao, Shaking table model test and numerical analysis of a supertall building with high-level transfer storey, Struct. Design Tall Spec. Build. 21 (10) (2012) 699–723, https://doi.org/10.1002/tal.632.
[8] E. Talebi, M.M. Tahir, F. Zahmatkesh, A.B.H. Kueh, Comparative study on the behaviour of buckling restrained braced frames at fire, J. Constr. Steel Res. 102 (2014) 1–12, https://doi.org/10.1016/j.jcsr.2014.06.003.
[9] M. Dehghani, R. Tremblay, Design and full-scale experimental evaluation of a seismically endurant steel buckling-restrained brace system, Earthq. Eng. Struct. Dyn. 47 (1) (2018) 105–129, https://doi.org/10.1002/eqe.2941.
[10] Y. Koetaka, H. Narihara, O. Tsujita, Experimental Study on Buckling Restrained Braces, Beijing, China, 2001.
[11] L.J. Jia, H. Ge, R. Maruyama, K. Shinohara, Development of a novel high-performance all-steel fish-bone shaped buckling-restrained brace, Eng. Struct. 138 (2017) 105–119, https://doi.org/10.1016/j.engstruct.2017.02.006.
[12] M. Gray, C. Christopoulos, J. Packer, D. Lignos, Development, validation, and modeling of the new cast steel yielding brace system, in: 20th Analysis and Computation Specialty Conference, American Society of Civil Engineers, Chicago, Illinois, United States, 2012, https://doi.org/10.1061/9780784412374.007.
[13] M. Gray, C. Christopoulos, J. Packer, Design and full-scale testing of a cast steel yielding brace system in a braced frame, J. Struct. Eng. 143 (4) (2017), https://doi.org/10.1061/(ASCE)ST.1943-541X.0001692.
[14] E.P. Popov, R.G. Black, Steel struts under severe cyclic loadings, J. Struct. Div. 107 (9) (1981) 1857–1881.
[15] C.C. Chou, S.Y. Chen, Subassemblage tests and finite element analyses of sandwiched buckling-restrained braces, Eng. Struct. 32 (8) (2010) 2108–2121, https://doi.org/10.1016/j.engstruct.2010.03.014.
[16] A. Maurya, M.R. Eatherton, R. Matsui, S.H. Florig, Experimental investigation of miniature buckling restrained braces for use as structural fuses, J. Constr. Steel Res. 127 (2016) 54–65, https://doi.org/10.1016/j.jcsr.2016.07.019.
[17] T. Gu, J.H. Li, J. Sun, L.J. Jia, T. Liu, H. Ge, Experimental study on miniature buckling-restrained brace with corrugated Core bar, J. Earthq. Eng. 26 (13) (2022) 6633–6655, https://doi.org/10.1080/13632469.2021.1927907.
[18] L.K. Helferich, Design and Experimental Evaluation of a Small-Scale Buckling Restrained Brace Analog, MS Thesis., University of Tennessee, Knoxville, 2021.
[19] P.C. Talley, Capacity Design Methods for Strongback Braced Frames, The University of Tennessee, Knoxville, 2018.
[20] B. Simpson, S. Mahin, Design development of a four-story Strongback braced frame, Key Eng. Mater. 763 (2018) 1050–1057, https://doi.org/10.4028/www.scientific.net/KEM.763.1050.
[21] Y.P. Gong, C.J. Hyde, W. Sun, T.H. Hyde, Determination of material properties in the Chaboche unified viscoplasticity model, Proc. Inst. Mech. Eng. Part L J. Mat. Design Appl. 224 (1) (2010) 19–29, https://doi.org/10.1243/14644207JMDA273.
[22] L.J. Jia, H. Kuwamura, Prediction of cyclic behaviors of mild steel at large plastic strain using coupon test results, J. Struct. Eng. 140 (2) (2014), https://doi.org/10.1061/(ASCE)ST.1943-541X.0000848.
[23] ASTM, Standard Test Methods for Tension Testing of Metallic Materials, ASTM International, West Conshohocken, Pennsylvania, 2021.
[24] AISC, Seismic Provisions for Structural Steel Buildings, 2016.